Solvothermal Synthesis of NiCo-Layered Double Hydroxide Nanosheets Decorated on RGO Sheets for High Performance Supercapacitor

Xiaoqing Cai, Xiaoping Shen, Lianbo Ma, Zhenyuan Ji, Chen Xu, Aihua Yuan

PII: S1385-8947(15)00101-1
DOI: http://dx.doi.org/10.1016/j.cej.2015.01.072
Reference: CEJ 13188

To appear in: *Chemical Engineering Journal*

Received Date: 5 November 2014
Revised Date: 3 January 2015
Accepted Date: 18 January 2015

Please cite this article as: X. Cai, X. Shen, L. Ma, Z. Ji, C. Xu, A. Yuan, Solvothermal Synthesis of NiCo-Layered Double Hydroxide Nanosheets Decorated on RGO Sheets for High Performance Supercapacitor, *Chemical Engineering Journal* (2015), doi: http://dx.doi.org/10.1016/j.cej.2015.01.072

Solvothermal Synthesis of NiCo-Layered Double Hydroxide Nanosheets Decorated on RGO Sheets for High Performance Supercapacitor

Xiaoqing Cai,[a] Xiaoping Shen,[a] Lianbo Ma,[a] Zhenyuan Ji,[a] Chen Xu,[a] and Aihua Yuan [b]*

[a] *School of Chemistry and Chemical Engineering, Jiangsu University, Zhenjiang 212013, People's Republic of China*

[b] *School of Environmental and Chemical Engineering, Jiangsu University of Science and Technology, Zhenjiang 212003, P. R. China*

** Corresponding author. Tel/Fax: +86-511-88791800.*

E-mail address: xiaopingshen@163.com (Xiaoping Shen).

ABSTRACT

Highly uniform composites composed of NiCo-layered double hydroxide (NiCo-LDH) and reduced graphene oxide (RGO) were successfully fabricated through a facile one-pot solvothermal method. The resulting composites (NiCo-LDH/RGO) display nanosheet architecture with tunable content of NiCo-LDH. By virtue of the greatly enhanced rate of electron and mass transfer as well as the improved specific surface area, the as-obtained NiCo-LDH/RGO composite electrodes exhibit excellent supercapacitive properties, and deliver a maximum specific capacitance of 1911.1 F g^{-1} at the current density of 2.0 A g^{-1}. Moreover, at the high current density of 20 A g^{-1}, the specific capacitance of NiCo-LDH/RGO nanocomposite still remains as high as 1469.8 F g^{-1}, indicating an extraordinary rate capability. Good cycling stability with the capacitance retention of 74% is obtained after repeating the charge-discharge measurements for 1000 cycles at the current density of 20 A g^{-1}. The combination of the high capacity of pseudocapacitive double hydroxides and good conductivity of RGO make the NiCo-LDH/RGO composites promising candidates for electrode materials in energy storage and conversion devices.

Keywords: Nickel cobalt layered double hydroxide; reduced graphene oxide; nanosheet; synthesis; supercapacitors

1. Introduction

In recent years, supercapacitor, as a promising energy storage and conversion device, has received intense attention due to its high power density, rapid charge/discharge rate, excellent cycle stability and high reliability [1,2]. Electrode materials, the main contributor of electrical energy storage of supercapacitors, have become the research hotspot in the energy storage field [3,4]. At present, three types of electrode materials have been widely utilized for supercapacitors: carbonaceous materials [5], metal oxides/hydroxides [6] and conducting polymers [7]. Carbonaceous materials store energy through charges adsorption in the electric double-layer of electrode/electrolyte interfaces, which suffer from the low energy density due to the inherent limitation of the electrostatic surface charging mechanism [8]. In contrast, metal oxides/hydroxides and conducting polymers conduct fast and reversible faradaic reactions at the interface of the electrode and the electrolyte, which contribute to better supercapacitive properties than carbonaceous materials [4]. However, conducting polymers in the long period of charge and discharge often produce the volume expansion and shrinking, which results in poor cycle stability [9]. In order to meet the demand for high performance energy storage and conversion devices, more and more researchers have focused on developing advanced pseudocapacitive materials based on transition-metal oxides/hydroxides.

Layered double hydroxides (LDHs) are a class of inorganic multi-metal clay materials that consist of metal cations in the host layer and ionic species in the interlayer space. LDHs can be expressed by a general chemical formula of

$[M^{2+}_{1-x}M^{3+}_{x}(OH)_2]^{x+}[A^{n-}_{x/n}]^{x-}\cdot mH_2O$, where M^{2+} and M^{3+} are divalent and trivalent cations and A^{n-} is charge-balancing anions of *n* valance [10,11]. Due to the large surface area with all atoms exposed and multiple oxidation states for reversible faradaic reactions, LDHs are regarded as the good candidates for supercapacitor electrode materials. Recently, transition-metal LDHs with excellent redox activity, flexible ion exchange ability, low cost and environmentally friendly nature have achieved significant progress for supercapacitor applications [12,13]. Especially, NiCo-LDHs with large interlayer spacings exhibit excellent electrochemical performances [14-19]. For instances, Hsu *et al.* prepared porous Ni-Co oxy-hydroxides with a specific capacitance of 636 F g^{-1} at current density of 2 A g^{-1} through a microwave-assisted hydrothermal annealing method [16]. Liu *et al.* synthesized nanostructured $Co_xNi_{1-x}(OH)_2$ composites onto nickel foam with a specific capacitance of 1464.7 F g^{-1} at current density of 1 A g^{-1} [18]. However, due to the hydrogen bonding interactions between the layered structures, NiCo-LDHs materials often show a low specific surface area resulting from the particle aggregation, which deteriorates the supercapacitive performance [19]. Moreover, the poor intrinsic electrical conductivity of NiCo-LDHs is also disadvantageous to its electrochemical performance [4]. To overcome these disadvantages is a key step to the practical application of NiCo-LDHs materials.

Recently, nanostructured carbon materials, mainly including carbon nanotubes (CNTs), carbon fiber and graphene, have been adopted to enhance the capacitive performance of LDHs materials [20-27]. For instance, Wang *et al.* fabricated

$Co_xNi_{1-x}(OH)_2$ coated on hollow carbon nanorod array through a facile electrodeposition process with discharge areal capacitance of 0.14 F cm^{-2} at 1 mA cm^{-2} [21]. Warsi *et al.* prepared conformal coating of CoNi-LDHs nanoflakes on carbon fibers with good electrochemical properties [22]. Especially, LDHs/graphene nanocomposites have been demonstrated to be promising electrode materials for supercapacitors [23-27]. Graphene possesses many unique properties such as extremely large surface area, excellent electron conductivity, good mechanical flexibility and high thermal/chemical stability, which supplies a perfect substrate for the growth of electrochemical active materials, and acts as an efficient current-collecting component for supercapacitor. For example, Wang et al. prepared graphene nanosheet/NiAl-LDHs composite with a maximum specific capacitance of 781.5 F g^{-1} at 5 mV s^{-1} [23]. Jin *et al.* fabricated CoAl-LDHs nanosheets attached on partial reduction of GO with a specific capacitance of 1204 F g^{-1} at 5 mV s^{-1} [24]. Hao *et al.* synthesized graphene/NiAl-LDH composite with a specific capacitance of 213.6 F g^{-1} at current density of 1 A g^{-1} [25]. Ma *et al.* prepared CoAl-LDH/RGO and CoNi-LDH/RGO superlattice composites with the specific capacitances of 450 and 650 F/g, respectively, at a current density of 5 A g^{-1} [26]. It was found that the combination of electrochemically active components with graphene to form graphene-based composites can effectively improve the capacitive performance due to the formation of conductive network and the increase of electrolyte contact area.

In this work, we report the fabrication of NiCo-LDH/RGO composites with NiCo-LDH porous nanosheets attached on reduced graphene oxide (RGO) sheets

through a facile one-pot solvothermal method. Unlike previously reported methods of LDH/RGO composites [28,29], no adscititious alkali sources are needed in the synthesis. In addition, graphene oxide (GO) was converted to RGO with methanol as the reducing agent, and no hazardous or toxic reductants such as hydrazine hydrate were used. More importantly, the as-prepared NiCo-LDH/RGO composites exhibit ultrahigh specific capacitance up to 1911.1 F g^{-1} at the current density of 2.0 A g^{-1}, and excellent rate capability with specific capacitance of 1469.8 F g^{-1} at current density of 20 A g^{-1}.

2. Experimental

2.1. Materials

Natural flake graphite with a particle size of 150 μm (99.9% purity) was purchased from Qingdao Guyu Graphite Co., Ltd. All of the other chemical reagents used in our experiments are of analytical grade, purchased from Sinopharm Chemical Reagent Co., Ltd, and used without further purification. Graphite oxide was synthesized from natural flake graphite using a modified Hummers method [30,31].

2.2. Synthesis of NiCo-LDH/RGO composites

The NiCo-LDH/RGO composites were prepared by a simple one-pot solvothermal method as follows. Typically, 1.0 g of cetyltrimethylammonium bromide (CTAB) and 30 mg of graphite oxide were dispersed in a mixed solvent containing 15 mL of methanol and 3 mL of deionized water by ultrasonication for 30 min to form a stable graphene oxide (GO) colloid. A solution of 0.84 mmol of

$Ni(NO_3)_2 \cdot 6H_2O$ and 0.56 mmol of $CoCl_2 \cdot 6H_2O$ (the molar ratio of $n(Ni(NO_3)_2 \cdot 6H_2O)/n(CoCl_2 \cdot 6H_2O) = 3/2$) dissolved in a mixed solvent of methanol (15 mL) and H_2O (3 mL) was slowly added into the GO dispersion under vigorous stirring at room temperature. After stirring for 1 h, the as-obtained suspension was transferred to a 60 mL Teflon-lined autoclave, which was then sealed and heated at 180 °C for 24 h. After being cooled to room temperature, the resultant products were centrifuged, washed with deionized water and absolute ethanol for several times to remove any impurities, and then dried in a vacuum oven at 45 °C for 24 h. For obtaining NiCo-LDH/RGO composites with different NiCo-LDH contents, the amount of $Ni(NO_3)_2 \cdot 6H_2O$ used in the synthesis was changed from 0.84 to 0.42, 0.63 and 1.05 mmol, respectively, and correspondingly the amount of $CoCl_2 \cdot 6H_2O$ was also changed to keep the molar ratio of Ni^{2+} to Co^{2+} to be 3:2. The final products were denoted as NiCo-LDH/RGO-1, NiCo-LDH/RGO-2, NiCo-LDH/RGO-3 and NiCo-LDH/RGO-4 for the initial feeding amount of 0.42, 0.63, 0.84 and 1.05 mmol of $Ni(NO_3)_2 \cdot 6H_2O$, respectively. For comparison, pure NiCo-LDH was synthesized in the absence of graphite oxide, and bare RGO was also prepared without $Ni(NO_3)_2 \cdot 6H_2O$ and $CoCl_2 \cdot 6H_2O$ but with the other experimental parameters constant.

2.3. Characterization

Powder X-ray diffraction (XRD) was performed on a Bruker D8 Advance diffractometer with Cu *K*α radiation (1.5406 Å) at a scanning rate of 7 °min^{-1}. The composition of the products was determined by energy-dispersive X-ray spectrometry

(EDS) and X-ray photoelectron spectroscopy (XPS, Thermo ESCALAB 250). The morphology and size of the products were examined by scanning electron microscopy (SEM, JSM-6480) and transmission electron microscopy (TEM, JEOL JEM-2100). Raman scattering was collected at room temperature using a DXR Raman spectrometer with 532 nm laser source. Fourier transform infrared (FT-IR) spectra were recorded on a Nicolet Nexus 470 spectrometer with KBr pellets. Brunauer-Emmett-Teller (BET) surface areas of the products were tested using a surface area and porosity analyzer (NDVA-2000e).

2.4. Electrochemical measurements

Electrochemical measurements were performed on a three-electrode setup using a CHI 760D electrochemical analyzer (Chen Hua Instruments, Shanghai, China) at room temperature. Platinum foil and saturated calomel electrode (SCE) were used as the counter and reference electrodes, respectively. The working electrodes were fabricated by mixing 80 wt% active materials (NiCo-LDH/RGO or NiCo-LDH), 10 wt% acetylene black and 10 wt% poly(vinylidene fluoride) (PVDF) binder in N-methyl-2-pyrrolidone solvent to form a homogeneous slurry, and then the slurry was coated on the nickel foam substrates (surface area 1 cm^2). After that, the nickel foam was placed into a vacuum oven and was dried at 80 °C for 48 h. The electrodes loaded with the active material were then pressed at 10 MPa. The masses of the electrodes are about 1.5, 2.0, 1.5, 2.0, 1.7 mg for NiCo-LDH/RGO-1, NiCo-LDH /RGO-2, NiCo-LDH/RGO-3, NiCo-LDH/RGO-4 and NiCo-LDH, respectively. The electrochemical properties of the as-prepared materials were evaluated by cyclic

voltammetry (CV), galvanostatic charge-discharge (CD) and electrochemical impedance spectroscopy (EIS) techniques in 3.0 M KOH aqueous solution at room temperature. The average specific capacitance was calculated from the galvanostatic CD curves according to the following equation [17,32]:

$$C_s = I\Delta t/(m\Delta V) \qquad (1)$$

where C_s is the specific capacitance (F g^{-1}) of the electrodes, I is the charge and discharge current (mA), Δt is the discharging time (s), m is the mass of the electroactive material of the electrode (mg), and ΔV is the discharging potential drop (V).

3. Results and discussion

3.1. Synthesis of NiCo-LDH/RGO composites

In this work, we prepared NiCo-LDH/RGO composites through a facile one-pot solvothermal method. As a result of oxygen-containing functional groups on the surface of GO sheets, GO is negatively charged, and therefore can adsorb positive ions and offer nucleation sites for the growth of nanoparticles [27]. When $Ni(NO_3)_2 \cdot 6H_2O$ and $CoCl_2 \cdot 6H_2O$ were added into GO suspension, the positively charged Ni^{2+} and Co^{2+} ions were absorbed on the surfaces of GO sheets through the electrostatic interactions. Hydroxyl ions can be produced slowly by the following redox reaction at 180 °C: $4CH_3OH + NO_3^- \rightarrow 4HCHO + NH_3 + OH^- + 2H_2O$ [33,34]. The hydroxyl ions reacted with Ni^{2+} and Co^{2+} ions to produce hydroxide monomers on the surface of GO, and then the monomers underwent olation reaction with each

other to form primary particles [35]. During this process, partial bivalent cobalt was converted to trivalent cobalt through high temperature oxidation [36]. As the primary particles aggregated gradually, they converted to nanosheets decorated on GO. The porosity of the nanosheets could be generated from the release of the ammonia gas during the synthesis. Meanwhile, GO was converted to RGO at the high temperature with methanol as the reducing agent [37]. Finally, NiCo-LDH/RGO composites with porous NiCo-LDH nanosheets attached on RGO sheets were obtained. The morphological evolution of the composite at different reaction time was investigated by SEM technique. It can be seen from Fig. S1 (see Supporting Information) that with the increasing reaction time, the product gradually evolved from flat nanosheets to highly wrinkled ones. We consider that in the hydrothermal process, the heat energy decreases the stability of the as-formed nanosheets, resulting in the crumpling of them so as to decrease the surface energy [38]. Meanwhile, the solvent deformation resulted from the high temperature and high pressure can also drive the collision, overlapping and cross-linking of the flexible nanosheets, which would contribute to the wrinkling of the nanosheets [38].

3.2. Structural and morphological characterization

XRD is conducted to characterize the phase structures of the as-synthesized materials. Fig. 1a shows the XRD patterns of graphite oxide, RGO, NiCo-LDH and NiCo-LDH/RGO-3. The diffraction pattern of graphite oxide exhibits a sharp peak centered at $2\theta = 10.3°$, which corresponds to the (001) reflection of graphite oxide [39]. The disappearance of the (001) peak and the emergence of a new diffraction peak at

2θ = 24° in the XRD pattern of RGO demonstrates that graphite oxide has been well reduced. The broad and weak peak at 2θ of about 13° in the XRD pattern of RGO originated from the SiO_2 substrate used in XRD measurement. The NiCo-LDH sample exhibits four characteristic diffraction peaks at 2θ values of 11.1°, 22.1°, 34.4° and 38.6°, which can be indexed to the (003), (006), (009) and (015) planes of hydrotalcite-like LDH phase [40]. The XRD pattern of NiCo-LDH/RGO-3 composite is similar to that of the pure NiCo-LDH, revealing the existence of NiCo-LDH in the composite. The disappearance of the peak at 24° suggests that in NiCo-LDH/RGO-3, the stacking of RGO sheets was well prevented due to the attachment of the NiCo-LDH nanosheets on them [41].

The EDS spectrum of NiCo-LDH/RGO-3 composite is presented in Fig. 1b. The elements of C, O, Co, Ni, Pt, Cl and Br are detected. The Pt signal comes from the plated element for SEM measurement, the carbon element comes from RGO, and the oxygen element derives from the residual oxygen-containing groups on RGO. The Cl and Br elements could come from Cl^- and Br^- anions, which act as charge-balancing ions and exist in the interlayer space of NiCo-LDH [42]. The atomic ratio of Ni to Co is found to be about 3 : 2, which is consistent with the initial molar ratio of Ni^{2+} to Co^{2+} used in the synthesis.

The chemical composition and surface chemical state of the NiCo-LDH/RGO-3 composite were investigated by XPS technique. The XPS survey spectrum of the NiCo-LDH/RGO-3 composite not only exhibits C 1s and O 1s peaks, but also shows the peaks corresponding to Ni 2p and Co 2p (Fig. 2a), well consistent with the

composition of NiCo-LDH/RGO-3. The C 1s XPS spectrum (Fig. 2b) can be deconvoluted into three different peaks centered at 284.5, 286.1 and 288.5 eV, corresponding to C-C, C-O and O=C-O groups, respectively [27]. The intensities of C-O and O=C-O peaks are remarkably weaker than that of C-C peak, further confirming the effective removal of oxygen-containing groups and the well reduction of GO into RGO during the hydrothermal process [43]. Fig. 2c shows the Ni 2p XPS spectrum, besides two shakeup satellites (indicated as "Sat"), there are two major peaks at 855.5 and 873.1 eV, corresponding to Ni $2p_{3/2}$ and Ni $2p_{1/2}$, respectively. The spin-energy separation of 17.6 eV is characteristic of Ni^{2+} in $Ni(OH)_2$ [44]. The Co 2p spectrum (Fig. 2d) can be fittted with two spin-orbit doublets and two shake-up satellites (identified as"Sat.") by using a Gaussian fitting method. One pair of binding energies centered at 780.2 and 795.6 eV corresponds to Co^{3+}, while the other pair at the higher energies of 782.1 and 796.6 eV is ascribed to Co^{2+}. These results indicate that there exist two kinds of cobalt oxidation state in the composite: i.e. Co^{2+} and Co^{3+} [15]. Based on the peak area calculation, the molar ratio of Co^{3+} to Co^{2+} is about 1:1, suggesting that about one half of Co^{2+} ions on the surface of NiCo-LDH/RGO-3 have been oxidized to Co^{3+}.

The morphology and microstructure of NiCo-LDH/RGO composites were characterized by TEM and SEM. Fig. 3 represents the typical (HR)TEM images of NiCo-LDH /RGO-3 composite. From Fig. 3a, it can be seen that the composite consists of numerous interconnected nanosheet, and the rippled and crumpled silk-like structure that RGO intrinsically own can be clearly seen. Fig. 3b reveals the perfect

combination of NiCo-LDH and RGO, in which NiCo-LDH nanosheets uniformly deposited on the surface of RGO sheets with a large contact area. NiCo-LDH nanosheets possess relatively rough surfaces, which make them easily differentiated from RGO sheets (Fig. 3b). The high-magnification TEM image (Fig. 3c) reveals the porosity of NiCo-LDH nanosheets, from which the pores can be clearly observed in the surface of the nanosheets. In addition, some small nanoparticles with dark contrast are also observed in the nanosheets. The inset of Fig. 3c shows the magnified view of a typical nanoparticle. The observed interplanar spacing of 0.23 nm matches well with the (015) lattice plane of NiCo-LDH, suggesting that the nanoparticles with dark contrast are NiCo-LDH. Fig. 3d shows HRTEM image of NiCo-LDH/RGO-3. The clear lattice fringes suggest the high crystallinity of the nanosheets, and the interplanar spacings of 0.26 and 0.23 nm match well with the (009) and (015) lattice planes of NiCo-LDH, respectively, further confirming the successful preparation of NiCo-LDH nanosheets. For comparison, TEM images of the as-synthesized pure NiCo-LDH product are presented in Fig. S2 (see Supporting Information). The pure NiCo-LDH product also shows porous nanosheet structure, which is similar to those observed in the NiCo-LDH/RGO composite. However, in the pure NiCo-LDH sample, the NiCo-LDH nanosheets show a severe agglomeration due to their strong stacking to decrease the surface energy. Nitrogen adsorption and desorption isotherms (Fig. S3, See Supporting Information) reveal that the specific surface areas of pure NiCo-LDH nanosheets and NiCo-LDH/RGO-3 composite are 7.5 and 27.4 m^2/g, respectively. This result demonstrates that the integration with RGO can significantly improve the

specific surface area of NiCo-LDH materials. The large specific area is in favor of the improvement of electrochemical performance by virtue of the more active surface of the active component accessible by the electrolyte [24]. SEM images of RGO, NiCo-LDH/RGO composites with different loading amounts of NiCo-LDH, and pure NiCo-LDH are presented in Fig. S4 (see Supporting Information). It can be seen that pure RGO nanosheets show relatively smooth lamellar structure (Fig. S4a, see Supporting Information), while NiCo-LDH/RGO composites display highly crumpled silk-like morphology with interconnected nanosheets (Fig. S4b-e, see Supporting Information). With the increasing NiCo-LDH content in the composites, the nanosheets interconnect more compactly. For pure NiCo-LDH (Fig. S4f, see Supporting Information), the nanosheets show severe agglomeration, which is well consistent with the TEM observation.

Raman spectroscopy is a powerful approach to characterize the structural properties of carbonaceous materials, such as the disorder and defect structures of graphene-based materials [23]. The typical Raman spectra of graphite oxide, RGO, NiCo-LDH and NiCo-LDH/RGO-3 composite are shown in Fig. 4. Except NiCo-LDH, all other samples display two prominent peaks at 1345 and 1596 cm^{-1}, which can be ascribed to the well documented D and G bands, respectively. The D band arises from structure defects and disorders that can break the symmetry and selection rule, while the G band derives from the E_{2g} phonon of C sp^2 atoms corresponding to stretching vibrations in the basal plane of graphene [45]. The integrated intensity ratio of D to G band (I_D/I_G) is often used as a measure of

structural defects and disorder in graphitic structures [46]. After the reduction of GO, the oxygen-containing functional groups in GO nanosheets are removed, and the conjugated graphene network (sp^2 carbon) with a smaller average size can be reestablished, which usually leads to an increment in the I_D/I_G value [47]. From Fig. 4a, an increment in I_D/I_G (1.87) is obtained for RGO as compared with that of graphite oxide (1.54), indicating that GO has been well deoxygenated and reduced during the synthesis process [23]. For NiCo-LDH/RGO-3 composite, a further increased I_D/I_G value (2.30) is obtained due to the presence of NiCo-LDH nanosheets, which would induce more defects and disorders [30]. In addition, the Raman spectra of NiCo-LDH and NiCo-LDH/RGO-3 composite show two peaks at 450 and 520 cm^{-1}, which correspond to Ni-O and Co-O vibrational modes, respectively [48,49]. Fig. 4b shows FT-IR spectra of graphite oxide, RGO, NiCo-LDH and NiCo-LDH/RGO-3 composite. As expected, the FT-IR spectrum of graphite oxide reveals the presence of oxygen-containing functional groups. In detail, the absorption bands at 3425 and 1423 cm^{-1} can be assigned to the stretching vibration and deformation vibration of O-H, respectively. The band at 1744 cm^{-1} belongs to the C=O stretching vibration of COOH groups. The stretching vibration peaks of C-OH and C-O are observed at 1235 and 1069 cm^{-1}, respectively. In addition, the band at 1622 cm^{-1} derives from the vibration of the adsorbed water molecules and/or the contribution of the skeletal vibration of unoxidized graphitic domains [30]. However, these peaks related with the oxygen-containing groups diminished or even vanished in the spectrum of RGO, which confirms the effective reduction of GO [30]. In the spectra of NiCo-LDH and

NiCo-LDH/RGO-3, the absorption peaks at 3583 and 1056 cm^{-1} can be ascribed to the stretching and deformation modes of MO-H (M represents Ni or Co) [49], and the absorption bands at 649 and 517 cm^{-1} derive from the stretching vibrations of Co-O and Ni-O, respectively [50,51]. In the spectrum of NiCo-LDH/RGO-3 composite, the absorption bands from the oxygen-containing groups almost disappear, further confirming the effective reduction of GO in NiCo-LDH/RGO-3 composite.

3.3. Electrochemical properties of the NiCo-LDH/RGO composites

The as-prepared NiCo-LDH/RGO composites were investigated as electrode materials for supercapacitors. We first carried out the CV measurements in a three-electrode system with 3.0 M KOH aqueous solution as the electrolyte. The shapes of CV curves (Fig. 5) clearly reveal the Faradaic characteristics of the as-prepared electrodes. Based on the CV curves, the specific capacitance of the electrodes can be calculated by the formula: $C_s = (\int IdV)/(vm\Delta V)$, where I is the response current, ΔV is the potential difference, v is the potential scan rate, and m is the mass of the active materials in the electrodes [14]. It can be seen that the specific capacitance is positively correlated with the mathematic area of CV curve at a fixed scan rate. Fig. 5a shows the CV curves of the NiCo-LDH/RGO composites and NiCo-LDH nanosheets at a scan rate of 40 mV s^{-1}. It can be seen that the mathematic areas of the CV curves of NiCo-LDH/RGO electrodes are larger than that of NiCo-LDH electrode, indicating that the NiCo-LDH/RGO electrodes possess higher specific capacitances. Fig. 5b exhibits the CV curves of NiCo-LDH/RGO-3 at different scan rates, ranging from 2 to 80 mV s^{-1}. Each CV curve exhibits a pair of

cathodic and anodic peaks, indicating the existence of faradic redox reactions during the CV tests [18]. With the increase of the scan rate, the anodic peak shifts positively and cathodic peak shifts negatively, accompanying with increasing current densities. The specific capacitances of NiCo-LDH/RGO-3 at the scan rate of 5, 10, 20, 40 and 80 mV s^{-1} are *ca*. 932.2, 834.8, 697.5, 551.8 and 411.1 F g^{-1}, respectively. The specific capacitances decrease with the increasing scan rate can be attributed to the limited diffusion rate of the alkali ions. When the scan rate increases, the rate of alkali ion transfer becomes relatively slow, and thus only the outer active surface of the electrode material can be utilized for charge storage during the redox process, resulting in a drop in specific capacitance [27]. For comparison, the CV curves of NiCo-LDH electrode at various scan rates and the corresponding capacitance changing curve are presented in Fig. S5 (see Supporting Information). The specific capacitances of NiCo-LDH at the scan rate of 5, 10, 20, 40 and 80 mV s^{-1} are *ca.* 444.7, 405.9, 342.9, 271.0 and 194.8 F g^{-1}, respectively, which reveals that the NiCo-LDH electrode has much smaller specific capacitance values than NiCo-LDH/RGO-3 electrode under the same scan rate.

To further illustrate the electrochemical performance of the as-prepared electrodes, galvanostatic charge-discharge measurements were conducted. Fig. 6a presents the typical charge-discharge curves of the NiCo-LDH/RGO composites and NiCo-LDH electrodes at the current density of 2.0 A g^{-1}. The existence of plateaus at around 0.2 V suggests the pseudocapacitive feature arising from the redox process of the electrodes [52], which is in good agreement with the CV curves (Fig. 5). The

specific capacitance can be calculated according to equation (1), the calculated specific capacitance values are *ca.* 1501.3, 1784.7, 1911.1, 1623.6 and 898.3 F g^{-1} for NiCo-LDH/RGO-1, NiCo-LDH/RGO-2, NiCo-LDH/RGO-3, NiCo-LDH/RGO-4 and NiCo-LDH electrodes, respectively. The large difference in the specific capacitances between NiCo-LDH/RGO composites and NiCo-LDH can be attributed to the existence of RGO in NiCo-LDH/RGO electrodes. Though RGO alone exhibits a small specific capacitance [20], it can largely contribute to the improvement of electrochemical performance of NiCo-LDH/RGO composites. On one hand, RGO can improve the conductivity of NiCo-LDH/RGO electrodes, which could enhance the charge transfer and charge transport necessary for relevant redox reactions [27]. On the other hand, RGO can act as an effective matrix for anchoring the NiCo-LDH nanosheets, which prevent the aggregation of the NiCo-LDH nanosheets and make them effectively accessible by electrolyte ions. Therefore, RGO in NiCo-LDH/RGO composites serve dual functions as both conductive channels and active interface centers. In addition, the optimal specific capacitance can be obtained through adjusting the molar ratio of NiCo-LDH to RGO. With the gradual increase of NiCo-LDH content in NiCo-LDH/RGO composites, the specific capacitances increase first and then decrease, and the NiCo-LDH/RGO-3 exhibits the largest specific capacitance among these composites. The increment of the specific capacitance can be attributed to the increased content of active material (NiCo-LDH) for capacitance generation. However, the increase of the NiCo-LDH content in NiCo-LDH/RGO composites will accordingly reduce the content of RGO, which

deteriorates the conductivity of the composites, and thus contributes to the decrease of the specific capacitance. Moreover, too high content of NiCo-LDH in the composites could increase the aggregation of NiCo-LDH nanosheets since some of them cannot well attach on RGO sheets, which results in a decreasing material utilization for capacitance generation.

Fig. 6b displays the charge-discharge curves of the NiCo-LDH/RGO-3 composite at various current densities. It can be seen that the discharge time decreases with the increase of the current density from 2.0 to 20 A g^{-1}. The specific capacitance values as a function of current density for NiCo-LDH/RGO-3 and NiCo-LDH electrodes are plotted in Fig. 6c. Both plots descend with the increasing current density. The specific capacitances of NiCo-LDH/RGO-3 electrode at 2.0, 3.0, 5.0, 10 and 20 A g^{-1} are 1911.1, 1900.0, 1890.0, 1698.4 and 1469.8 F g^{-1}, respectively. This suggests that almost 76.9% of the specific capacitance at 2.0 A g^{-1} is retained when the current density is increased to 20 A g^{-1}, which is much higher than that of NiCo-LDH (55.7%), suggesting a better rate capability of NiCo-LDH/RGO-3 electrode.

Electrochemical stability was evaluated by repeating the galvanostatic charge-discharge measurement for 1000 cycles at a constant current density of 20 A g^{-1}. Fig. 6d exhibits the specific capacitance as a function of cycle number and the inset displays the charge-discharge curves of the initial 10 cycles. It can be seen that the specific capacitance shows a gradual decrease at first and then it remains nearly constant after 400 cycles. At the 1000th cycle, there is still 74% capacitance retention

for the NiCo-LDH/RGO-3 electrode, indicating a good cycling stability. For comparison, the cycling stability of NiCo-LDH electrode is shown in Fig. S6 (see Supporting Information). It can be seen that the specific capacitance shows a continuous decrease and only 51% capacitance retention is obtained at the 1000th cycle, suggesting that the cycling stability of NiCo-LDH electrode is much poorer than that of NiCo-LDH/RGO electrode. This result demonstrates that the introduction RGO into NiCo-LDH can significantly improve the electrochemical stability of NiCo-LDH.

Fig. 7 shows the resistance characteristics of NiCo-LDH/RGO-3, NiCo-LDH and RGO electrodes investigated by EIS measurements. The equivalent circuit that employed to fit the EIS spectra is presented in the inset of Fig. 7, where R_s represents the resistance related to the ionic conductivity of the electrolyte and electronic conductivity of the electrodes and current collectors, Q is the constant phase element accounting for a double-layer capacitance, R_{ct} is the charge-transfer resistance associated with the Faradic reactions, W is the Warburg resistance arised from the ion diffusion and transport in the electrolyte, and C_L is the limit capacitance [21,23]. R_s can be valued from the intercept at the real axis in the high-frequency region. Based on the fitting values calculated from the equivalent circuit, the R_s (1.41 ohm) of NiCo-LDH/RGO-3 composite is lower than that of NiCo-LDH (1.67 ohm) and RGO (1.56 ohm). In addition, NiCo-LDH/RGO-3 and NiCo-LDH consist of a semi-arc in the high frequency region and a straight line in the low frequency region. The diameter of the arc corresponds to the charge transfer resistance (R_{ct}). The larger

semi-arc diameter suggests the larger resistance of electrochemical reaction between the electrode and electrolyte [9]. The fitting R_{ct} (0.24 ohm) of NiCo-LDH/RGO-3 electrode shows much smaller value than that of NiCo-LDH (0.75 ohm), indicating that the charge transfer resistance for NiCo-LDH/RGO-3 electrode is much smaller than that for NiCo-LDH one. This result confirms that the electrochemical resistance of NiCo-LDH could be greatly reduced by incorporating with RGO sheets [27]. Besides, compared with NiCo-LDH electrode, NiCo-LDH/RGO-3 electrode has a more vertical line in the low frequency region, suggesting a lower Warburg impedance [27]. These results well coincide with the CV and discharge results, which confirm that NiCo-LDH/RGO-3 has much better electrochemical performance than NiCo-LDH.

4. Conclusions

Highly uniform composites with NiCo-LDH nanosheets attached on RGO sheets have been successfully fabricated by a facile one-pot solvothermal method. The as-synthesized NiCo-LDH/RGO composites exhibit excellent electrochemical performance with high specific capacitance and rate capability, good charge/discharge stability and long cycle life. The extraordinary electrochemical performance can be attributed to the porous layered architecture of NiCo-LDH/RGO composites as well as the effective combination between NiCo-LDH nanosheets and RGO sheets. It is revealed that RGO not only acts as conductive channel to improve the conductivity of the composites but also as an ideal matrix to prevent NiCo-LDH nanosheets from

agglomerating. This work provides a facile and effective route to fabricating graphene-based bimetallic LDHs electrode materials for supercapacitor applications.

Acknowledgements

The authors are grateful for financial support from Specialized Research Fund for the Doctoral Program of Higher Education of China (No. 20123227110018) and National Nature Science Foundation of China (No. 51272094).

References

[1] J. Yan, Q. Wang, T. Wei, Z.J. Fan, Recent advances in design and fabrication of electrochemical supercapacitors with high energy densities, Adv. Energy Mater. 4 (2014) 1300816.

[2] S. Han, D.Q. Wu, S. Li, F. Zhang, X.L. Feng, Porous graphene materials for advanced electrochemical energy storage and conversion devices, Adv. Mater. 26 (2014) 849-864.

[3] G.P. Wang, L. Zhang, J.J. Zhang, Crumpled nitrogen-doped graphene nanosheets with ultrahigh pore volume for high-performance supercapacitor, Chem. Soc. Rev. 41 (2012) 797-828.

[4] X. Wang, C.Y. Yan, A. Sumboja, J. Yan, P.S. Lee, Achieving high rate performance in layered hydroxide supercapacitor electrodes, Adv. Energy Mater. 4 (2014) 1301240.

[5] Y.W. Zhu, S. Murali, M.D. Stoller, K.J. Ganesh, W.W. Cai, P.J. Ferreira, A. Pirkle R.M. Wallace, K.A. Cychosz, M.Thommes, D.Su, E.A. Stach, R.S. Ruoff, Carbon-based supercapacitors produced by activation of graphene, Science 332 (2011) 1537-1541.

[6] L. Wang, Y.J. Hao, Y. Zhao, Q.Y. Lai, X.Y. Xu, Hydrothermal synthesis and electrochemical performance of NiO microspheres with different nanoscale building blocks, J. Solid State Chem. 183 (2010) 2576–2581.

[7] H.L. Wang, Q.L. Hao, X.J. Yang, L.D. Lu and X. Wang, Graphene oxide doped polyaniline for supercapacitors, Electrochem. Commun. 11 (2009) 1158-1161.

[8] F.Z. Deng, L. Yu, G. Cheng, T. Lin, M. Sun, F. Ye, Y.F. Li, Synthesis of ultrathin mesoporous $NiCo_2O_4$ nanosheets on carbon fiber paper as integrated high-performance electrodes for supercapacitors, J. Power Sources 251 (2014) 202-207.

[9] N.T.H. Trang, H.V. Ngoc, N. Lingappan, D.J. Kang, A comparative study of supercapacitive performances of nickel cobalt layered double hydroxides coated on ZnO nanostructured arrays on textile fibre as electrodes for wearable energy storage devices, Nanoscale 6 (2014) 2434-2439.

[10] J. S. Valente, M. Sanchez-Cantu, E. Lima and F. Figueras, Method for large-scale production of multimetallic layered double hydroxides: Formation mechanism discernment, Chem. Mater. 21 (2009) 5809-5818.

[11] Q. Wang, D. O'Hare, Recent advances in the synthesis and application of layered double hydroxide (LDH) nanosheets, Chem. Rev. 112 (2012) 4124-4155.

[12] F.Z. Zhang, Y. Zhang, C.L. Yue, R. Zhang, Y.M. Yang, Facile fabrication of spherical architecture of Ni/Al layered double hydroxide based on in situ transformation mechanism, AIChE J. 60 (2014) 4027-4036.

[13] W. Hong, J.Q. Wanga, L.Y. Niua, J.F. Suna, P.W. Gong, S.R. Yang, Controllable synthesis of CoAl LDH@$Ni(OH)_2$ nanosheet arrays as binder-free electrode for supercapacitor applications, J. Alloys Compd. 608 (2014) 297-303

[14] J.C. Chen, C.T. Hsu, C.C. Hu, Superior capacitive performances of binary nickel-cobalt hydroxide nanonetwork prepared by cathodic deposition, J. Power Sources 253 (2014) 205-213.

[15] H. Chen, L.F. Hu, M. Chen, Y. Yan, L.M. Wu, Nickel-cobalt layered double hydroxide nanosheets for high-performance supercapacitor electrode materials. Adv. Funct. Mater. 24 (2014) 934-942.

[16] H.Y. Hsu, K.H. Chang, R.R. Salunkhe, C.T. Hsu, C.C. Hu, Synthesis and characterization of mesoporous Ni-Co oxy-hydroxides for pseudocapacitor application, Electrochim. Acta 94 (2013) 104-112.

[17] J. Pu, Y. Tong, S.B. Wang, E. Sheng, Z.H. Wang, Nickel-cobalt hydroxide nanosheets arrays on Ni foam for pseudocapacitor applications, J. Power Sources 250 (2014) 250-256.

[18] X.W. Liu, J.C. Huang, X.P. Wei, C.L. Yuan, T. Liu, D.X. Cao, J.L. Yin, G.L. Wang, Preparation and electrochemical performances of nanostructured $Co_xNi_{1-x}(OH)_2$ composites for supercapacitors, J. Power Sources 240 (2013) 338-343.

[19] M.F. Warsia, I. Shakir, M. Shahid, M. Sarfraz, M. Nadeemd, Z.A. Gilani, Conformal coating of cobalt-nickel layered double hydroxides nanoflakes on carbon fibers for high-performance electrochemical energy storage supercapacitor devices, Electrochim. Acta 135 (2014) 513-518.

[20] J.W. Zhao, J. Chen, S.M. Xu, M.F. Shao, Q. Zhang, F. Wei, J. Ma, M. Wei, D.G. Evans, X. Duan, Hierarchical NiMn layered double hydroxide/carbon nanotubes architecture with superb energy density for flexible supercapacitors, Adv. Funct. Mater. 24 (2014) 2938-2946.

[21] L. Wan, J.W. Xiao, F. Xiao, S. Wang, Nanostructured (Co, Ni)-based compounds coated on a highly conductive three dimensional hollow carbon nanorod array (HCNA) scaffold for high performance pseudocapacitors, ACS Appl. Mater. Interfaces 6 (2014) 7735-7742.

[22] M.F. Warsia, I. Shakir, M. Shahid, M. Sarfraz, M. Nadeemd, Z.A. Gilani, Conformal coating of cobalt-nickel layered double hydroxides nanoflakes on carbon fibers for high-performance electrochemical energy storage supercapacitor devices, Electrochim. Acta 135 (2014) 513-518.

[23] Z. Gao, J. Wang, Z.S. Li, W.L. Yang, B. Wang, M.J. Hou, Y. He, Q. Liu, T. Mann, P.P Yang, M.L. Zhang, L.H. Liu, Graphene nanosheet/Ni^{2+}/Al^{3+} layered double-hydroxide composite as a novel electrode for a supercapacitor, Chem. Mater. 23 (2011) 3509-3516.

[24] X.Y. Dong, L. Wang, D. Wang, C. Li, J. Jin, Layer-by-layer engineered Co-Al hydroxide nanosheets/graphene multilayer films as flexible electrode for

supercapacitor, Langmuir 28 (2012) 293-298.

[25] Z. Wang, X. Zhang, J.H. Wang, L.D. Zou, Z.T. Liu, Z.P. Hao, Preparation and capacitance properties of graphene/NiAl layered double-hydroxide nanocomposite, J. Colloid Interface Sci. 396 (2013) 251-257.

[26] R.Z. Ma, X.H. Liu, J.B. Liang, Y.S. Bando, T. Sasaki, Molecular-scale heteroassembly of redoxable hydroxide nanosheets and conductive graphene into superlattice composites for high-performance supercapacitors, Adv. Mater. 26 (2014) 4173-4178.

[27] Y. Wimalasiria, R. Fan, X.S. Zhao, L.D. Zou, Assembly of Ni-Al layered double hydroxide and graphene electrodes for supercapacitors, Electrochim. Acta 134 (2014) 127-135.

[28] S. Werner, V.W.H. Lau, S. Hug, V. Duppel, H. Clausen-Schaumann, B.V. Lotsch, Cationically charged $Mn^{II}Al^{III}$LDH nanosheets by chemical exfoliation and their use as building blocks in graphene oxide based materials, Langmuir 29 (2013) 9199-9207.

[29] B. Li, Y.F. Zhao, S.T. Zhang, W. Gao, M. Wei, Visible-light-responsive photocatalysts toward water oxidation based on NiTi-layered double hydroxide/reduced graphene oxide composite materials, ACS Appl. Mater. Interfaces 5 (2013) 10233-10239.

[30] Z.Y. Ji, X.P. Shen, J.L. Yang, G.X. Zhu, K.M. Chen, A novel reduced graphene oxide/Ag/CeO_2 ternary nanocomposite: Green synthesis and catalytic properties, Appl. Catal., B 144 (2014) 454-461.

[31] W.S. Hummers, R.E. Offeman, Preparation of graphitic oxide, J. Am. Chem. Soc. 80 (1958) 1339-1339.

[32] F. He, Z.B. Hu, K.Y. Liu, S.R. Zhang, H.T. Liu, S.B. Sang, In situ fabrication of nickel aluminum-layered double hydroxide nanosheets/hollow carbon nanofibers composite as a novel electrode material for supercapacitors, J. Power Sources 267 (2014) 188-196.

[33] Y. Ren, L. Gao, From three-dimensional flower-like α-$Ni(OH)_2$ nanostructures to hierarchical porous NiO nanoflowers: Microwave-assisted fabrication and supercapacitor properties, J. Am. Ceram. Soc. 93 (2010) 3560-3564.

[34] X.F. Sun, X.Q. Qiu, L.P. Li, G.S. Li, ZnO twin-cones: Synthesis, photoluminescence, and catalytic decomposition of ammonium perchlorate, Inorg. Chem. 47 (2008) 4146-4152.

[35] H. Chen, S.X. Zhou, L.M. Wu, Porous nickel hydroxide-manganese dioxide-reduced graphene oxide ternary hybrid spheres as excellent supercapacitor electrode materials, ACS Appl. Mater. Interfaces 6 (2014) 8621-8630.

[36] R.Z. Ma, J.B. Liang, X.H. Liu, T. Sasaki, General insights into structural evolution of layered double hydroxide: Underlying aspects in topochemical transformation from brucite to layered double hydroxide, J. Am. Chem. Soc. 134 (2012) 19915-19921.

[37] D.R. Dreyer, S. Murali, Y.W. Zhu, R.S. Ruoff, C.W. Bielawski, Reduction of graphite oxide using alcohols, J. Mater. Chem. 21 (2011) 3443-3447.

[38] S. Bai, X.P. Shen, G.X. Zhu, A.H. Yuan, J. Zhang, Z.Y. Ji, D.Z Qiu, The influence of wrinkling in reduced graphene oxide on their adsorption and catalytic properties, Carbon 60 (2013) 157-168.

[39] Z. Wang, X. Zhang, J.H. Wang, L.D. Zou, Z.T. Liu, Z.P. Hao, Preparation and capacitance properties of graphene/NiAl layered double-hydroxide nanocomposite, J. Colloid Interface Sci. 396 (2013) 251-257.

[40] J.C. Huang, T. Lei, X.P. Wei, X.W. Liu, T. Liu, D.X. Cao, J.L. Yin, G.L. Wang, Effect of Al-doped β-$Ni(OH)_2$ nanosheets on electrochemical behaviors for high performance supercapacitor application, J. Power Sources 232 (2013) 370-375.

[41] Z.Y. Ji, G.X. Zhu, X.P. Shen, H. Zhou, C.M. Wu, M. Wang, Reduced graphene oxide supported FePt alloy nanoparticles with high electrocatalytic performance for methanol oxidation, New J. Chem. 36 (2012) 1774-1780.

[42] F. Cavani, F. Trifirò, A. Vaccari, Hydrotalcite-type anionic clays: Preparation, properties and applications, Catal. Today 11 (1991) 173-301.

[43] Y.X. Xu, K.X. Sheng, C. Li, G.Q. Shi, Self-assembled graphene hydrogel via a one-step hydrothermal process, ACS Nano, 4 (2010) 4324-4330.

[44] H. Wang, X. Xiang, F. Li, Facile synthesis and novel electrocatalytic performance of nanostructured Ni-Al layered double hydroxide/carbon nanotube composites, J. Mater. Chem. 20 (2010) 3944-3952.

[45] F. Tuinstra, J.L. Koenig, Raman spectrum of graphite, J. Chem. Phys. 53 (1970) 1126-1130.

[46] M.S. Dresselhaus, A. Jorio, M. Hofmann, G. Dresselhaus, R. Saito, Perspectives

on carbon nanotubes and graphene raman spectroscopy, Nano Lett. 10 (2010) 751-758.

[47] C. Gómez-Navarro, R.T. Weitz, A.M. Bittner, M. Scolari, A. Mews, M. Burghard, K, Kern, Electronic transport properties of individual chemically reduced graphene oxide sheets, Nano Lett. 7 (2007) 3499-3503.

[48] J. Memon, J.H. Sun, D.L. Meng, W.Z. Ouyang, M.A. Memon, Y. Huang, S. Yan, J.X. Geng, Synthesis of graphene/Ni-Al layered double hydroxide nanowires and their application as an electrode material for supercapacitors, J. Mater. Chem. A 2 (2014) 5060-5067.

[49] J.T. Kloprogge, R.L. Frost, Fourier transform infrared and raman spectroscopic study of the local structure of Mg-, Ni-, and Co- hydrotalcites, J. Solid State Chem. 146 (1999) 506-515.

[50] M. Srivastava, M.E. Uddin, J. Singh, N.H. Kim, J.H. Lee, Preparation and characterization of self-assembled layer by layer $NiCo_2O_4$-reduced graphene oxide nanocomposite with improved electrocatalytic properties, J. Alloys Compd. 590 (2014) 266-276.

[51] Y.R. Ren, H.M. Wei, X.B. Huang, B. Yang, J.W. Wang, J.N. Ding, Fabrication of NiO nanowires/G composite as electrode material for high performance supercapacitor, Int. J. Electrochem. Sci. 9 (2014) 7206-7216.

[52] L. Yan, R.Y. Li, Z.J. Li, J.K. Liu, Y.J. Fang, G.L. Wang, Z.G. Gu, Three-dimensional activated reduced graphene oxide nanocup/nickel aluminum layered double hydroxides composite with super high

electrochemical and capacitance performances, Electrochim. Acta 95 (2013) 146-154.

Figure captions

Fig. 1. (**a**) XRD patterns of graphite oxide, RGO, NiCo-LDH and NiCo-LDH/RGO-3 composite; (b) EDS spectrum of NiCo-LDH/RGO-3 composite.

Fig. 2. XPS spectra of NiCo-LDH /RGO-3 composite: (a) survey spectrum, (b) C 1s, (c) Ni 2p and (d) Co 2p.

Fig. 3. (a-c) TEM images and (d) HRTEM image of NiCo-LDH/RGO-3 composite.

Fig. 4. (a) Raman spectra of graphite oxide, RGO, NiCo-LDH and NiCo-LDH/RGO-3 composite. (b) FT-IR spectra of graphite oxide, RGO, NiCo-LDH and NiCo-LDH /RGO-3 composite.

Fig. 5. (a) CV curves of NiCo-LDH/RGO composites and NiCo-LDH electrodes at scan rate of 40 mV s^{-1}; (b) CV curves of NiCo-LDH/RGO-3 composite electrode at different scan rates.

Fig. 6. (a) Charge-discharge curves of NiCo-LDH/RGO composites and NiCo-LDH electrodes at the current density of 2.0 A g^{-1}; (b) Charge-discharge curves of NiCo-LDH/RGO-3 electrode at various current densities; (c) the specific capacitance values of NiCo-LDH/RGO composites and NiCo-LDH electrodes as a function of current densities; (d) the cycling performance of NiCo-LDH/RGO-3 electrode at a constant current density of 20 A g^{-1}. The inset of (d) exhibits the charge-discharge curves of the initial 10 cycles.

Fig. 7. EIS of NiCo-LDH/RGO-3, NiCo-LDH and RGO electrodes.

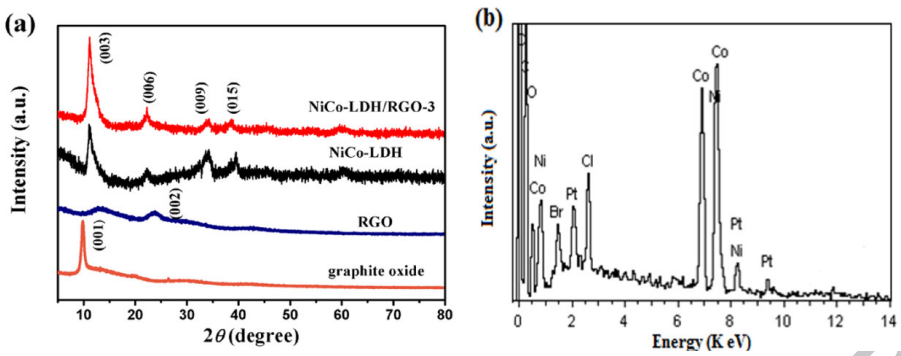

Figure 1

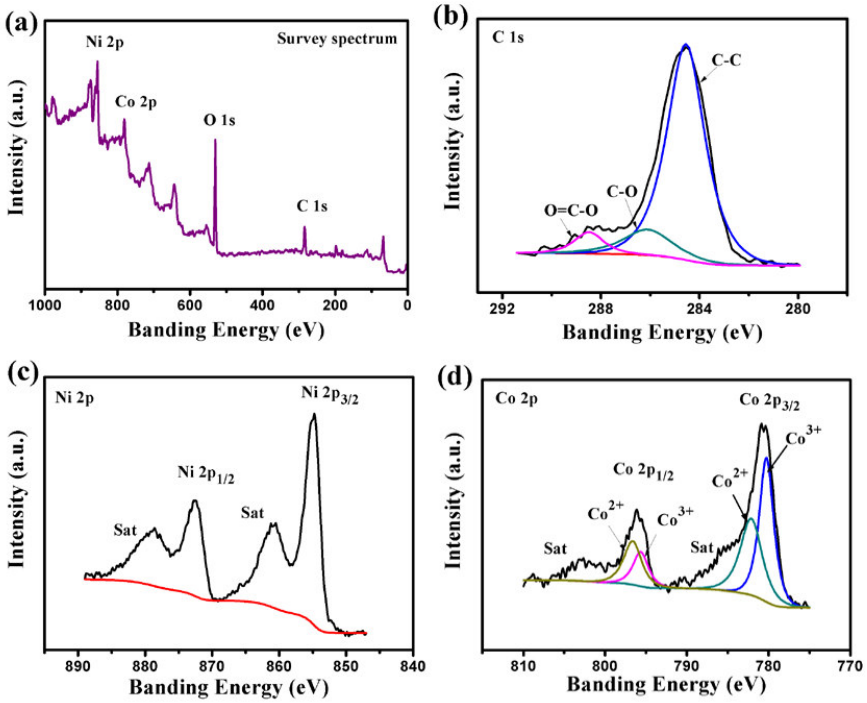

Figure 2

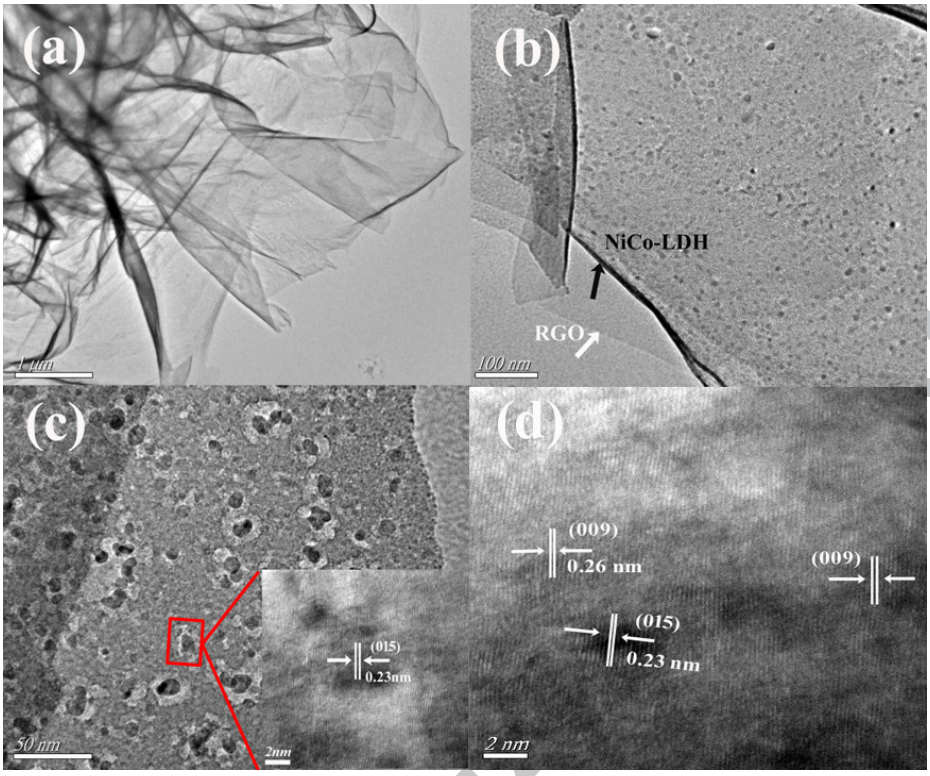

Figure 3

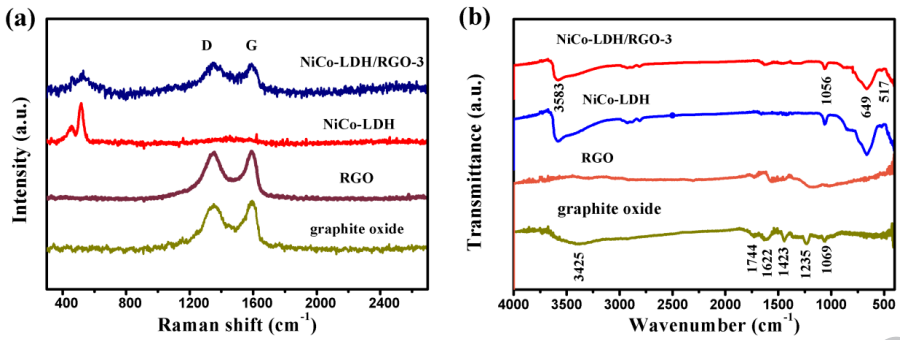

Figure 4

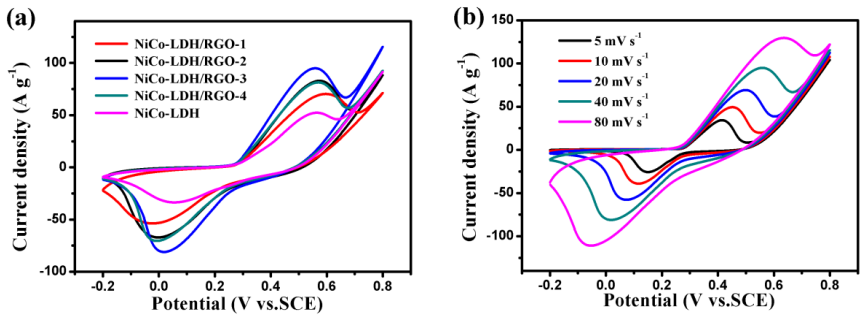

Figure 5

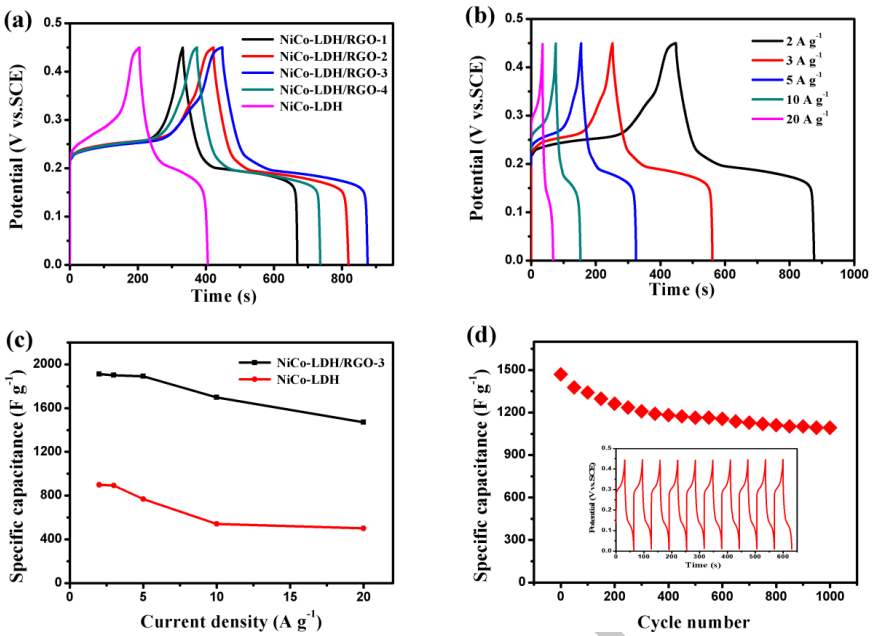

Figure 6

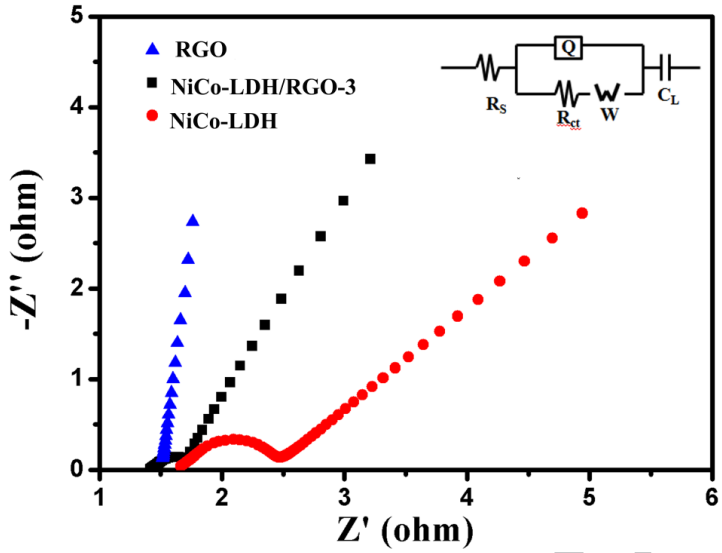

Figure 7

- Ni-Co LDH/RGO composites were synthesized through a facile solvothermal approach.
- Porous Ni-Co LDH nanosheets decorated on RGO sheets homogeneously.
- The Ni-Co LDH/RGO composite exhibits excellent capacitive performance.
- Possible mechanism for the enhanced capacitive performance was proposed.